Effective Separation and Recovery of Manganese and Potassium from Biomass Ash by Solvent Extraction

Sylwia Oleszek,* Kenji Shiota, Minhsuan Chen, and Masaki Takaoka

ACCESS | Metrics & More | Article Recommendations

ABSTRACT: Manganese (Mn) is considered an important, energy-critical metal due to its leading role in the production of electrochemical energy storage devices. One valuable source of Mn is hyperaccumulator plants used for the phytoremediation of contaminated soil. In this study, stems and leaves of ginger (*Zingiber officinale*), which accumulate Mn at moderate levels (∼0.2 wt %) and potassium (K) at high levels (>5 wt %), were analyzed to assess the potential of recovering metals from this plant. The extraction behaviors of Mn and K were studied using raw and ash samples (100−600 °C). It was crucial to set an appropriate incineration temperature (300 °C) to selectively extract K (∼96%) and Mn (∼90%) using water and nitric acid over two consecutive steps. Additionally, citric acid, a cost-effective and environmentally friendly solvent, was just as effective (∼85%) as nitric acid in extracting Mn. X-ray absorbance near-edge spectroscopy and X-ray diffraction analysis of the ash before and after extractions were applied to elucidate the extraction mechanism. The results revealed that selective extraction of both compounds was possible due to the change in the oxidative state of Mn(II) (soluble in water) into Mn(III) and Mn(IV) (insoluble in water) during sample incineration. Simultaneously, there were complex reactions associated with the changes within potassium carbonate compounds; however, these did not affect the K extraction efficiency.
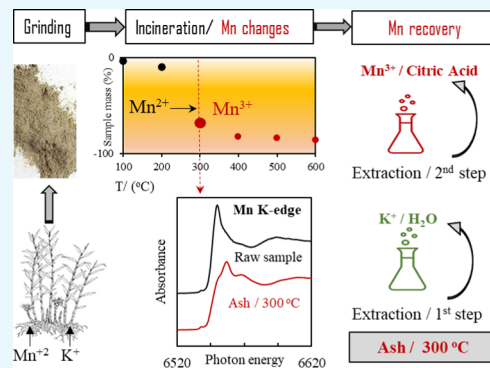
INTRODUCTION

Manganese (Mn) is a critical element required for various low-carbon technologies. For example, Mn plays a leading role in the production of electrochemical energy storage (EES) devices, such as lithium-ion batteries, which are used extensively in electric vehicles, portable electronics, and smart grids.[1] In addition to EES, Mn is important in the advancement of carbon and capture storage (CCS) technology,[1] as well as for the development of renewable energy resources (e.g., geothermal, solar, and wind).[2] Mn is also essential for iron and steel production;[3] therefore, it is critical to ensure a stable supply of this metal. According to World Bank predictions for 2013−2050,[3] the cumulative demand for Mn will increase by 2590% under the 2DS scenario (i.e., 2 °C increase in global temperature) compared to the 6DS scenario because of the high need for CCS related to gas and coal use. Considering that the Mn has no satisfactory substitute in its major application, it will enforce increased recyclability efforts for this and the other critical metals from end-of-life products; however, it is unlikely to be sufficient to cover all the Mn demand.[4] The Mn annual production rate and reserve are 18 and 62 million metric tons, respectively. Mn is mainly extracted from Mn ores with a minimum elemental content of 5−15%, with most ores being of considerably higher grade, up to 45% Mn.[2,5]

Mn is abundant in the soil. Some plants[6−11] can accumulate Mn in their shoots at concentrations of at least 10,000 mg·kg^{-1}

dry weight. These Mn-hyperaccumulating plants could be used to help meet the market demand for Mn. There are only 10−20 plant species that hyperaccumulate Mn and they can be found in Australia, New Caledonia, China, Malaysia, and Japan. These species can be specifically applied in contaminated areas for soil phytoremediation (e.g., near mining areas).[10−12] Overall, Mn-hyperaccumulating plants show potential in the development of phytomining techniques and may serve as a stable source of high-quality Mn.

Similar to Mn, K is a critical micronutrient in plant growth. Almost 90% of the K compounds produced (mainly KCl) are used as fertilizers in the agricultural sector.[13,14] Although industrial sources of K are limited, K from crop residues can partially substitute for K fertilizer to fulfill crop requirements. This can help reduce fertilizer expenses and promote soil and crop-related benefits.[15] The demand for K (as K_2O) increased by approximately 2.4% from 2015 to 2020 and is forecasted to increase further.[16,17]

© 2022 The Authors. Published by American Chemical Society

20155

https://doi.org/10.1021/acsomega.2c02002
ACS Omega 2022, 7, 20155−20164

Table 1. Elemental Composition of the Collected Dry Samples Analyzed by the Portable XRF

wt %	Si	P	S	Cl	K	Ca	Rb	Zn	Sr
max	0.310	0.183	0.446	0.623	13.9	4.02	0.059	0.065	0.009
min	0.043	0.018	0.118	0.040	4.19	0.310	0.005	0.003	0.002
average	0.128	0.088	0.222	0.202	8.93	1.23	0.020	0.012	0.003
median	0.110	0.091	0.213	0.166	8.99	1.08	0.019	0.008	0.003
SD	0.061	0.041	0.058	0.117	2.27	0.675	0.010	0.011	0.002
RSD	47.6	46.8	26.0	57.8	25.4	54.8	51.5	91.9	49.4
detected	123	114	130	130	130	130	130	79	86
wt %	Ti	Mg	Mn	Fe	Cu	Zr	Cd	Sn	Sb
max	0.011	0.319	0.205	0.028	0.015	0.002	0.003	0.003	0.002
min	0.007	0.190	0.019	0.019	0.008	0.002	0.002	0.002	0.002
average	0.009	0.267	0.059	0.024	0.012	0.002	0.002	0.003	0.002
median	0.009	0.270	0.046	0.025	0.012	0.002	0.002	0.003	0.002
SD	0.002	0.044	0.0431	0.0046	0.0049	1E-18	0.0003	0.0007	0
RSD	17.8	16.5	72.7	19.1	43.0	7E-14	13.7	28.3	0
detected	6	11	25	3	2	24	46	2	2

For the aforementioned reasons, it is vital to develop an efficient recovery method for K from biomass waste to enable sustainable circulation and supply of the micronutrient. In recent years, global interest in recovering K from biomass ash has been increasing. For example, K in different forms has been successfully recovered from rice,[18] wheat straw,[19] husk coffee waste,[4] and tropical fruit waste (e.g., empty palm fruit bunches, banana peels, and corncobs[20] ash). By contrast, there is a limited study[21] on the recovery of Mn from biomass ash.

Hence, we established a simple, low-cost, solvent-based, and non-time-consuming method for efficiently extracting and separating Mn and K from ginger crop waste. The extraction behaviors of Mn and K with various solvents and extraction conditions (temperature and time) were examined, such as incinerating ginger crop waste at various temperatures (100–600 °C). The forms of Mn and K obtained from raw and ash samples at selected temperatures (300 and 600 °C) were characterized using X-ray absorption spectroscopy (XAS) and X-ray diffraction (XRD). The total concentrations of Mn and K were quantified using an inductively coupled plasma atomic emission spectrometer (ICP-AES) and an ICP mass spectrometer (ICP-MS).

2. MATERIAL AND METHODS

2.1. Material. Dry and milled samples ($n = 130$) of ginger leaf and caulome were provided by the Kochi Agricultural Technology Center (Japan). The elemental compositions of the samples were characterized with X-ray fluorescence (XRF) using a portable instrument (Niton XL3t-950S, Thermo Fisher Scientific). The average composition across all samples is provided in Table 1.

Samples with the highest amounts of Mn (Table 2) were selected for a series of extraction experiments.

Extrapure HNO_3 (60 and 70%), HCl (35%), and acetic acid (AA; CH_3COOH, 99%) were purchased from Nacalai Tesque (Japan). H_2SO_4 (95%), H_2O_2 (30−35%), and citric acid (CA; $HOC(CO_2H)(CH_2CO_2H)_2$, granular powder) were obtained from Wako Pure Chemistry Co. (Japan). Ultrapure water was used for the analyses (Milli-Q gradient, Merck, Germany).

2.2. Experimental Methods. *2.2.1. Thermogravimetric Analysis (TGA).* The thermal behaviors of selected raw samples (Table 2) were assessed using a Rigaku Thermo Plus TG 8120 analyzer (Japan). Approximately, 10 mg of each sample was placed into an open alumina pan and heated from room

Table 2. Comparison of the K and Mn in the Selected Samples Quantified by Different Methods[a]

sample (S)	quantification method	K	Mn
		wt (%)	
S1	XRF	7.19	0.03
		4.40	0.05
S2	XRF	9.61	0.11
	ICP-MS	5.60	0.10
S3	XRF	7.16	0.03
	ICP-MS	3.70	0.04
S4	XRF	5.22	0.21
	ICP-MS	2.80	0.14
S5	XRF	5.09	0.03
	ICP-MS	2.80	0.04
ICP-MS/LOD[b]	20		0.05

[a]The ICP-MS values were used for the extraction recovery calculation (eq 1). [b]LOD: limit of detection.

temperature to 600 °C at a constant rate of 10 °C·min⁻¹ in air. Based on the thermal profiles obtained from TGA, the incineration temperatures were determined.

2.2.2. Sample Incineration. For each individual raw sample (Tables 2), 1 g of material was weighed, placed in a crucible, and then transferred to a muffle furnace (Isuzu Cap VTDW-16R, Japan). The furnace was heated dynamically until the desired temperature (100, 200, 300, 400, 500, or 600 °C) was reached, and the temperature was maintained for 2 h. After cooling, the crucible with the residue was weighed again. The particle size of the selected incinerated samples (S2, S4, and S5; Table 2) at 300 and 600 °C was determined based on the laser diffraction and scattering method using SALD-2300 (Shimadzu, Japan). The particles size of ashes (300 °C) was 36.164 μm (S2), 58.304 μm (S4), and 69.449 μm (S5), while the particles size of ashes (600 °C) was 30.735 μm (S2), 35.813 μm (S4), and 34.404 μm (S5), respectively.

2.2.3. Extraction. Different extraction procedures (Figure 1) were applied to selected raw and ash samples.

2.2.3.1. Acid Digestion. This procedure was performed by EMATEC Co. (Japan) to quantify the total amounts of K and Mn in the raw samples (Table 2). Briefly, 1 g of each individual sample was digested with a 1:2 (v/v) mixture of HNO_3 and HCl on a hot plate (HTP552AB, Advantec, Japan). Next, $HClO_4$ was applied to decompose the sample completely. The obtained
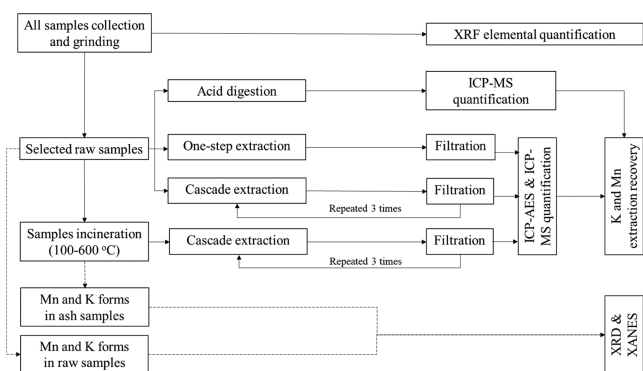
Figure 1. Experimental procedures for the quantification and characterization of the K and Mn in raw and ash samples.

solutions were diluted and analyzed using ICP-MS (7800 ICP-MS, Agilent Technologies, Inc.).

2.2.3.2. One-Step Extraction. Approximately, 0.3 g of each raw sample was placed into a glass flask. Next, approximately 80 mL of solvent was added to the sample, and the solution was agitated using a magnetic stirrer at a controlled temperature. After this extraction process, the extract solution was filtered through a membrane filter (cellulose mixed ester type, pore size 0.2 μm, Advantec) into a volumetric flask, into which ultrapure water was added until a final volume of 100 mL was attained. One-step extraction was performed using ultrapure water or HNO$_3$, HCl, H$_2$SO$_4$, AA, or CA as acid solvents at concentrations of 0.01 or 0.1 M. Extractions were conducted over two different time durations (1 or 5 h) and at two temperatures (30 or 70 °C). Extractions using water and HNO$_3$ as solvents were performed in triplicate (for both temperatures and extraction times); extractions using other solvents were performed once for each set of conditions. In terms of measurement repeatability, standard deviations of 0.9 and 5.9% were obtained for water and HNO$_3$, respectively.

2.2.3.3. Cascade Extraction. Cascade extraction was performed for raw and ash samples. Generally, the procedure was similar to that for the one-step extraction, but extraction took place over three steps instead of one: ultrapure water in the first step and 0.01 and 0.1 M HNO$_3$ in the next two. Each extraction time step was 1 h, and the extraction temperature was 30 °C. Additionally, instead of HNO$_3$, extraction was performed with 0.1 M CA for selected ash samples. Cascade extraction was performed twice for all samples.

K and Mn contents in individual extracts from the one-step and cascade extraction processes were quantified using an ICP-AES (iCAP7400 Duo, Thermo Fisher Scientific). Mn was also measured using an ICP-MS (XSeries 2 Xt, Thermo Fisher Scientific). Standard solutions of K and Mn at different concentrations were prepared for calibration, and yttrium (Y) was used as an internal standard. The calibration solutions were prepared using individual 1000 mg·L^{-1} K, Mn, and Y solutions (FUJIFILM Wako Chemical, Japan). ICP-AES and ICP-MS measurements were repeated three times for each sample. The relative standard deviation varied from 0.2 to 2.0%.

The recovery rate (R_M) of an individual metal (M) from one-step and cascade extractions was calculated as follows

$$R_M = (C_M \times V/M \times W_M) \times 100\% \qquad (1)$$

where C_M is the analyzed metal concentration in an extract [mg·L^{-1}], V is the total volume of the extract [L], M is the mass of the

sample [g], and W_M is the initial weight of the metal in the raw sample [wt %].

2.2.4. Characterization of Raw and Ash Samples. Raw and ash samples (300 and 600 °C) before and after extractions were characterized by the XRD (RINT Ultima+PC 220, Rigaku) using Cu Kα1 radiation (1.54059 Å). XAS was applied to analyze the oxidative state of K and Mn in selected raw and ash samples (before extraction). K K-edge and Mn K-edge X-ray absorption near-edge structure (XANES) experiments were conducted with the beamlines BL-11B and BL-12C, respectively (Photon Factory, Japan). Powdered samples were mounted on a probe using carbon tape before being placed in a chamber. K K-edge XANES spectra were collected between 3560 and 3700 eV in total electron yield and fluorescence yield modes. Mn K-edge XANES spectra were collected between 6200 and 6800 eV. Individual reference materials were mixed with boron nitride and compacted into pellets that were then analyzed in the transmission mode.

3. RESULTS AND DISCUSSION

3.1. Elemental Composition of Ginger Crop Waste. As shown in Table 1, K had the highest content among various detected elements in the ginger crop waste, with an average value of 8.93 wt % and a maximum value of 13.9 wt %, indicating that the ginger crop waste is a rich source of this element. Some samples also contained high levels of Mn, with a maximum value of 0.205 wt % as revealed by XRF analysis. Among the collected samples, the five with the highest Mn contents were selected for extraction experiments (samples S1−S5 in Table 2).

3.2. Incineration of the Ginger Crop Waste Samples. The samples S1−S5 (Table 2) were incinerated at different temperatures and the obtained residue amounts (average values from at least two runs) are shown in Figure 2A. For comparison, the average thermal profile of the samples incinerated by TGA is shown in Figure 2B. Incineration at 100 °C and 200 °C
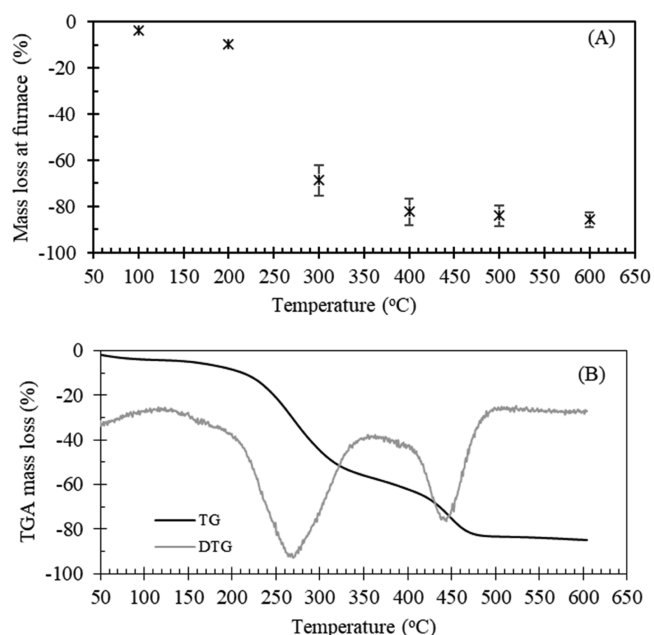

Figure 2. Mass loss (average values and standard deviation) for the samples (S1−S5, Table 2) incinerated at isothermal conditions using a muffle furnace (A). The average thermal profile of the samples incinerated at the dynamic conditions using the TGA (B).
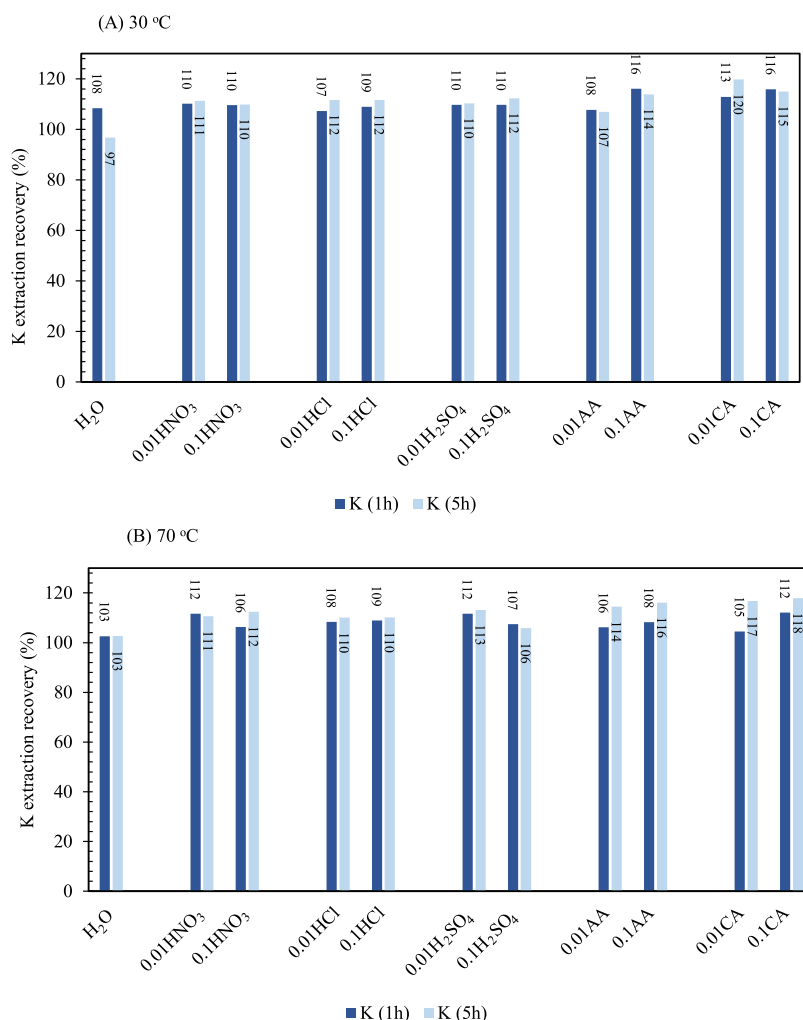
Figure 3. Effect of solvent type and concentration, extraction time, and temperature on K recovery at 30 °C (A) and 70 °C (B) from the raw sample (S1, Table 2) in the one-step extraction.

decreased the sample weight slightly, by 4 and 10%, respectively. This weight change was associated with the vaporization of moisture (up to 150 °C) and the initial degradation of organic matter (at 200 °C). These mass losses corresponded well to those observed in TGA (Figure 2B). A marked decrease in sample weight—by 70%) was observed at 300 °C (Figure 2A).

This was likely due to intensive organic matter degradation and vaporization of organic compounds.[22,23] This mass loss was reflected by the wide derivative thermogravimetry (DTG) peak (Figure 2B) between 200 and 350 °C. Incineration of samples at 400 °C resulted in a further decrease in weight (Figure 2A), with the decrease reflected by a second DTG peak between 400 and 500 °C (Figure 2B). This mass loss might have been due to the progressive degradation of organic matter and eventual decomposition of oxalates (e.g., CaC_2O_4, Na_2CO_3, and $K_2C_2O_4$), as reported by Deka and Neog.[24] A maximum decrease in sample weight (by 86%) was obtained at 600 °C and it was comparable to that incinerated at 500 °C (Figure 2). The raw and incinerated samples were subjected to a different extraction process as shown in Figure 1.

3.3. Raw Samples in One-Step Extraction: Influence of Solvent Type and Molarities and Extraction Conditions (Temperature and Time) on K and Mn Extraction Recovery. The extraction efficiencies of K and Mn from a selected raw sample (S1, Table 2) using various solvents and extraction conditions are shown in Figures 3 and 4, respectively. For K (Figure 3A,B), the maximum extraction efficiency was over 100% for almost all solvents used, and the acid molarity (0.01 or 0.1 M), extraction time (1 or 5 h), and temperature (30 or 70 °C) had negligible impacts on the amount of K recovered. Overestimation of the extraction efficiency (eq 1) could have resulted from the different analytical methods applied for K quantification (ICP-AES and ICP-MS).

For Mn, the extraction efficiency fluctuated between 33 and 98% depending on the solvent used (Figure 4A,B). The lowest values were obtained when water was used, and the extraction efficiency was comparable under different extraction conditions (33−38%). When strong acids (HNO_3, HCl, or H_2SO_4) were used, the extraction efficiency ranged from 75 to 89% at 30 °C and from 80 to 98% at 70 °C (Figure 4). Between the two weak acids (AA or CA) used, the Mn extraction was substantially more efficient with CA (0.1 M), with an extraction efficiency comparable to those obtained using strong acids. Increasing the molarity of the weak acids from 0.01 to 0.1 M also significantly improved the Mn extraction efficiency. Based on these results, the cascade extraction conditions for raw and ash samples were set to an extraction time of 1 h and temperature of 30 °C with 0.01/0.1 M HNO_3 and 0.1 M CA used as solvents.

3.4. Ash Samples in a Three-Step (Cascade) Extraction: Influence of Incineration Temperatures on K and Mn
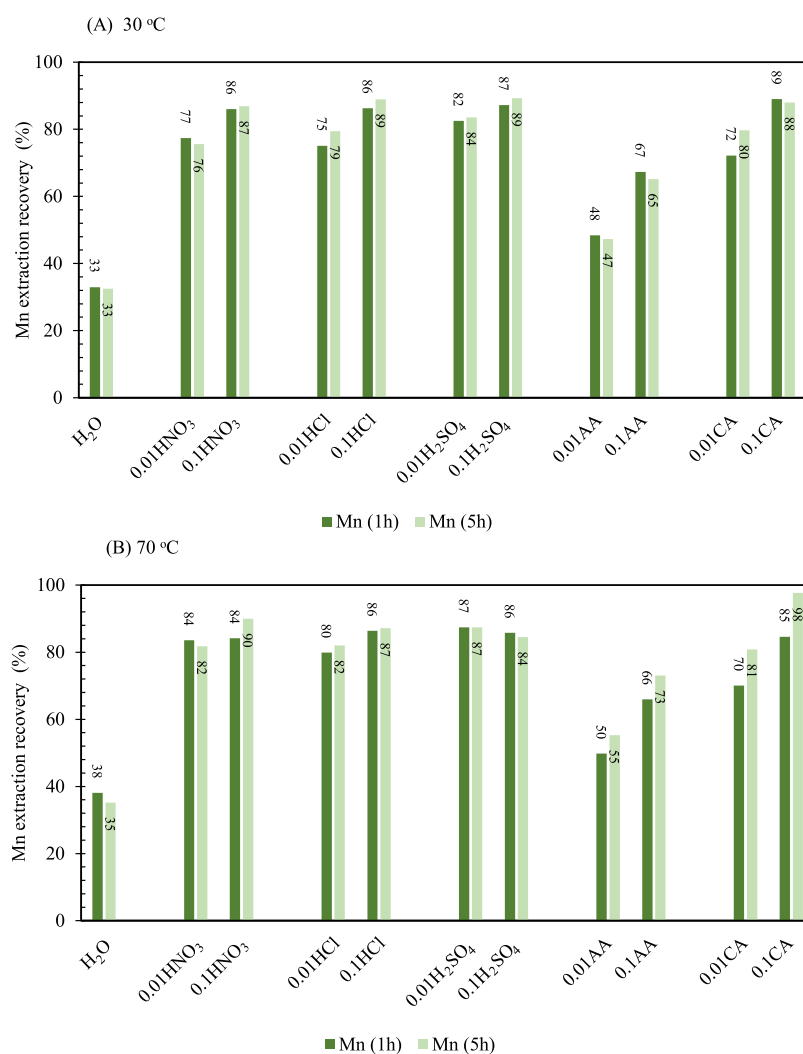
Figure 4. Effect of solvent, solvent concentration, time, and temperature on Mn recovery at 30 °C (A) and 70 °C (B) from the raw sample (S1, Table 2) in the one-step extraction.

Extraction Recovery from Ashes. Selected ash and raw samples (S2–S5, Table 2) were processed in a three-step extraction, with water (E1), 0.01 M HNO_3 (E2), and 0.1 M HNO_3 (E3) used as the respective solvent at each step. The average extraction efficiencies for K and Mn are shown in Figure 5A,B, respectively.

As can be seen in Figure 5A, the extraction efficiency of K was not significantly influenced by the sample incineration temperature. The extraction efficiency at the first step (E1) was 96–108% using water (Figure 5A). In the second step (E2) using acid, the K recovery rate ranged between 3 and 11%.

In contrast to K, the incineration temperature significantly influenced the extraction behavior of Mn (Figure 5B). The total extraction efficiency of Mn from raw and ash samples incinerated at 100 °C was approximately 70–76%. Half of the Mn extracted was obtained in the first step (E1) using water, with the other half obtained in the second step (E2) using an acid. The extraction efficiency of Mn from ash obtained after incineration at 200 °C with water was comparable (40%) to those from raw and ash samples treated at 100 °C. The extraction efficiency at E2 (with acid) increased to approximately 66%. With incineration temperatures of 300 and 400 °C, the extraction efficiency of Mn with water was approximately 11 and 4%, respectively, whereas more than 90–92% of the Mn was

extracted with HNO_3 at E2. For samples incinerated at higher temperatures (500 and 600 °C), the recovery rate of Mn decreased to below 60%, and most of the extraction took place at the second (E2) and third (E3) steps (Figure 5B). The results indicate that, for samples incinerated at 300 and 400 °C, it is possible to extract K at the first step using water with an efficiency of 96 ± 6.0 and 100 ± 5.5%, respectively. In the following extraction steps using acid, it is then possible to extract Mn with an efficiency of 90 ± 6.0 and 92 ± 6.0%, respectively.

Ashes received from the incineration of sample S1 (Table 2) at 100 or 300 °C were extracted following a similar procedure, but using 0.1 M CA in the second step (E2). From ash remaining after incineration at 300 °C, the K and Mn extraction efficiencies (103 ± 1.0 and 85 ± 9.0%, respectively) were comparable with those obtained using 0.01 M HNO_3 (Figure 6). Sample incineration at 300 °C or higher makes it possible to selectively extract K and Mn using different solvents. Moreover, Mn can be efficiently extracted using a cost-effective solvent (CA) that is also environmentally friendly compared to HNO_3.

3.5. Characteristics of K and Mn Compounds in Raw and Ash Samples and in Residues Before and After Extraction. The normalized XANES K-edge spectra for raw and ash samples and selected reference K compounds are shown in Figure 7. In the spectra for raw samples, a wide shoulder (*a*)
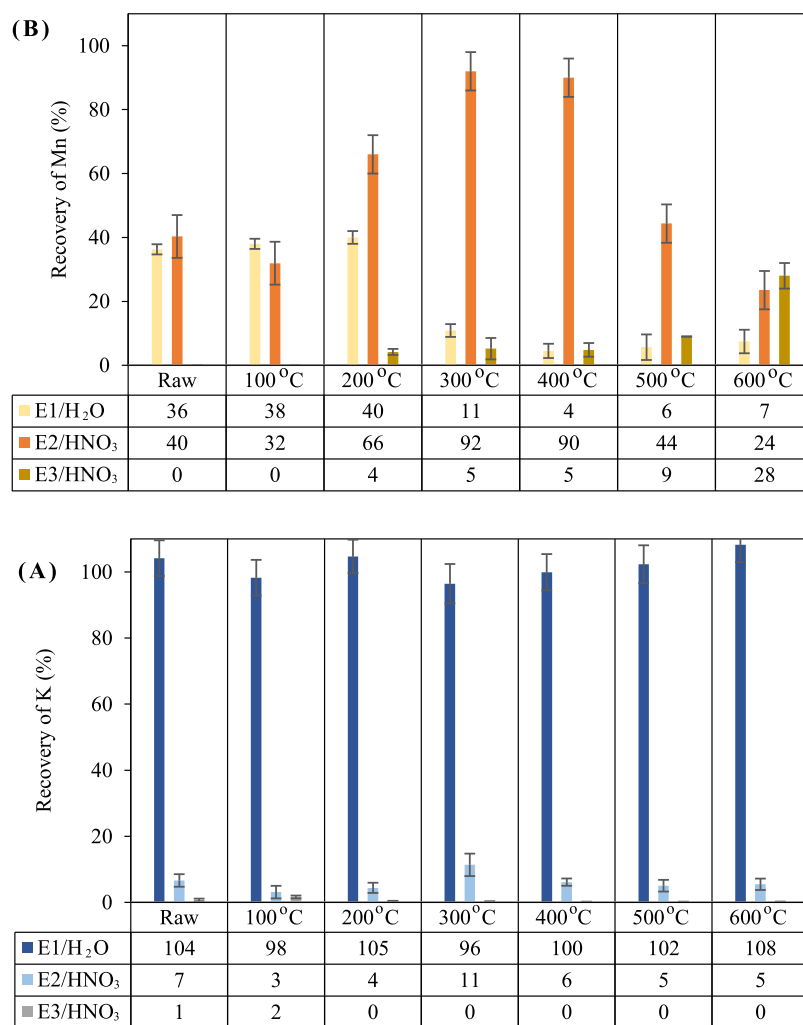
Figure 5. Recovery of K (A) and Mn (B) from the raw and ash samples (S2−S5, Table 2) in consecutive three-step extraction (E1−E3). Error bars are the standard deviations.
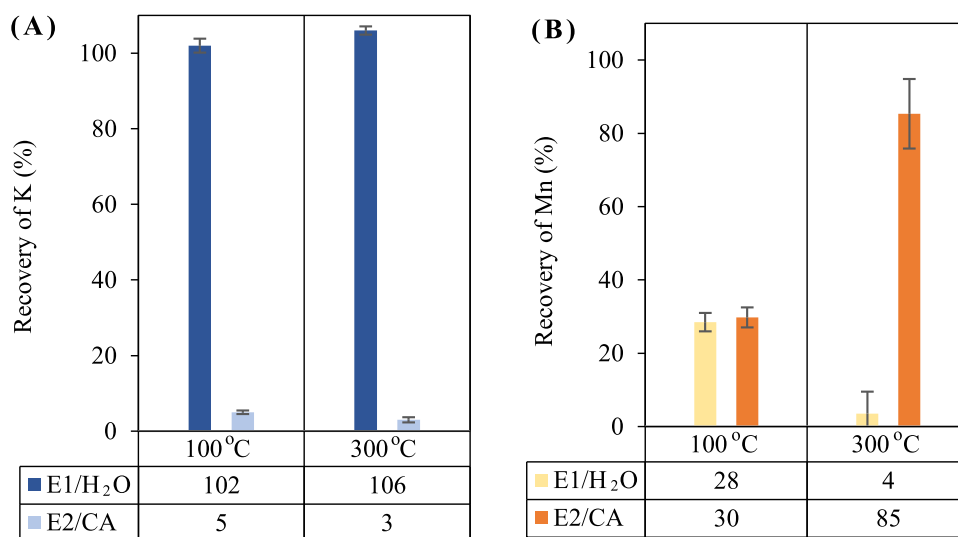

Figure 6. Recovery of K (A) and Mn (B) from the ash sample (S1, Table 2) in the consecutive two-step extraction (E1, E2). Error bars are the standard deviations.

was observed in the 3605−3606 eV range, as well as very small peaks at 3608−3609 eV (*b*) and 3613−3614 eV (*c*) (Figure 7A). The intensity of the *b* and *c* peaks increased markedly for

samples incinerated at 300 and 600 °C (Figure 7B,C). Based on comparisons with the reference compounds, it was deduced that the shoulder at the low-energy region (*a*) represents K
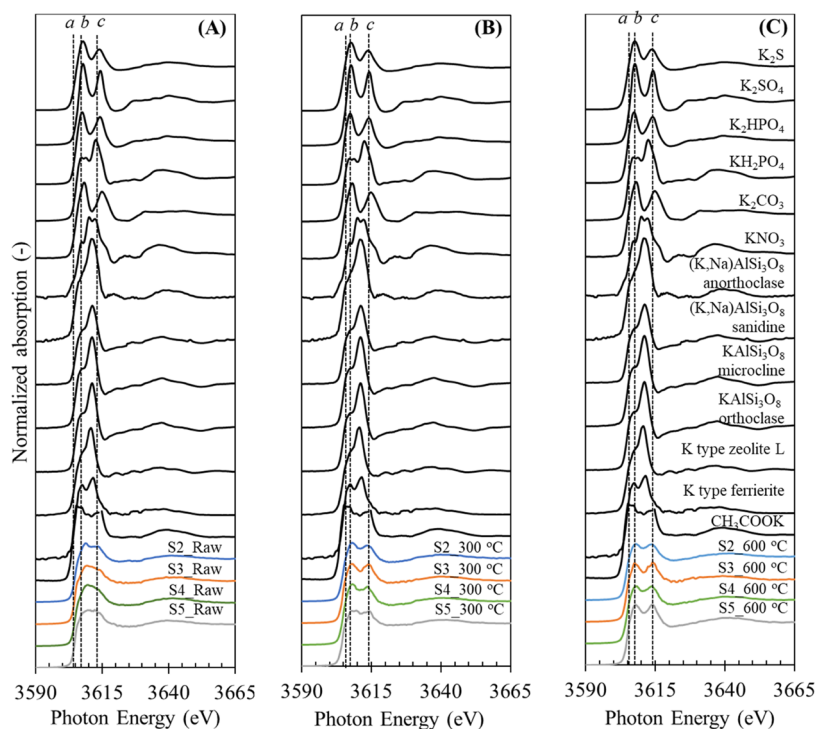
Figure 7. Normalized K K-edge XANES spectra of the raw samples (S2−S5, Table 2) (A) and their ashes at 300 °C (B) and 600 °C (C) in comparison with reference compounds.
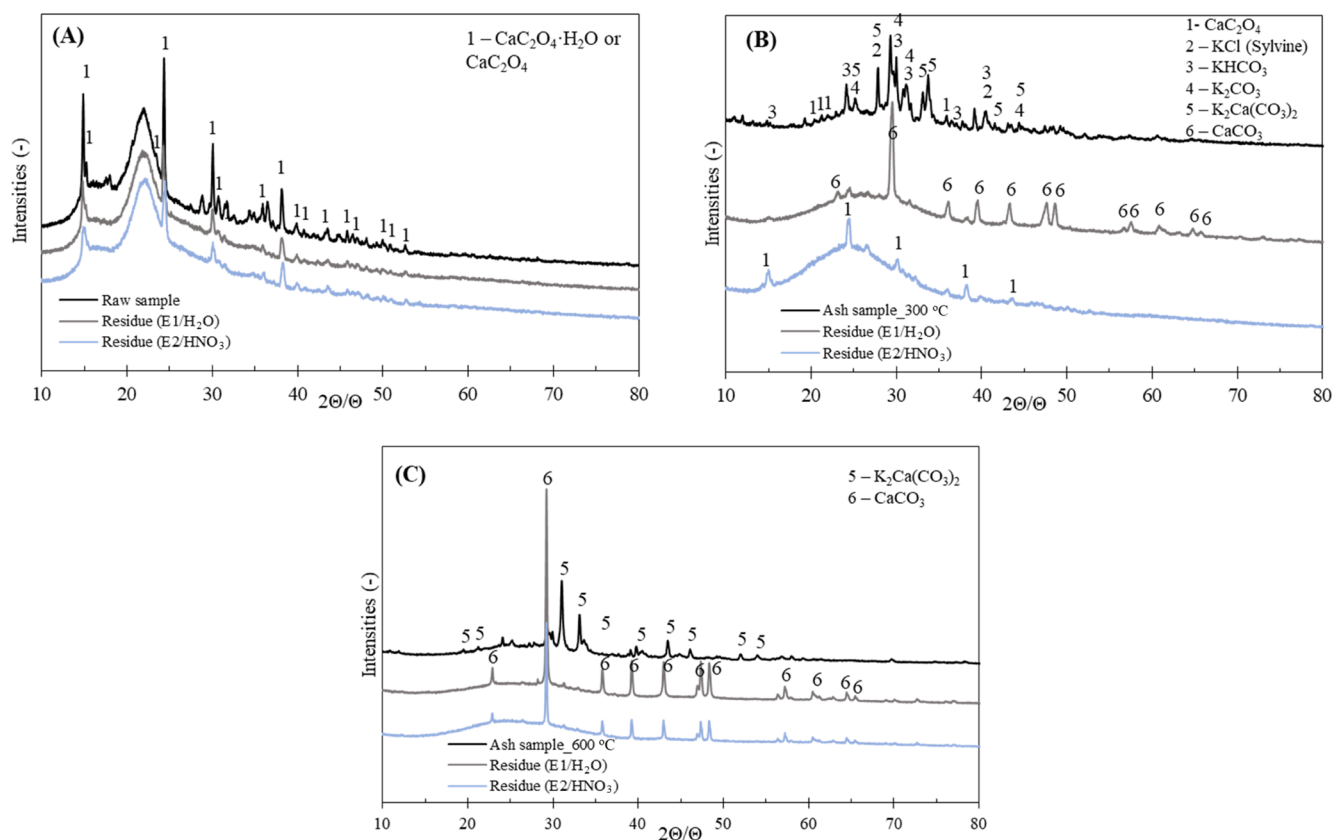

Figure 8. Characteristic of the raw (A) and ash samples obtained at 300 °C (B) and 600 °C (C) and the appropriate extractions (E1, E2) residues by XRD.

coexisting with Si−O forms, whereas the b and c peaks correspond to various K compounds containing sulfide, sulfate, carbonate, and phosphate.[25] Detailed XRD characterization of

the samples (Figure 8) confirmed the XANES results, revealing carbonates as the predominant compounds in the ash generated
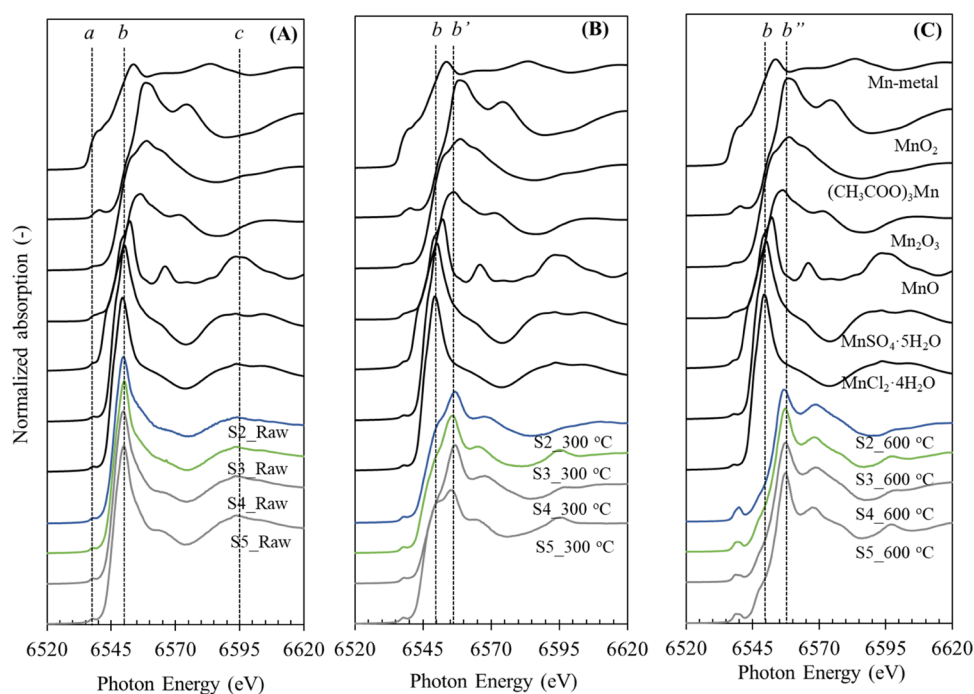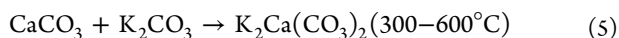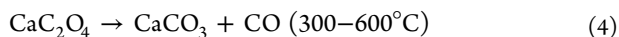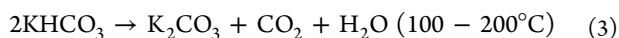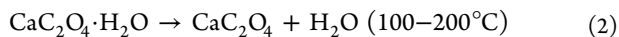
Figure 9. Normalized Mn K-edge XANES spectra of the raw samples (S2−S5, Table 2) (A) and their ashes at 300 °C (B) and 600 °C (C) in comparison with reference compounds.

at 300 °C (K_2CO_3, $KHCO_3$, and $K_2Ca(CO_3)_2$) and 600 °C ($K_2Ca(CO_3)_2$).

The spectrum for raw samples (Figure 8A) exhibited peaks representing hydrated calcium oxalate (CaC_2O_4). The patterns observed for changes and forms of K carbonates in the studied samples (Figure 8) agree well with those reported by Thyler;[22] namely, CaC_2O_4 was found to be the prevalent phase in untreated Scots pine powder, whereas double carbonates (present in two polymorphs: bütschliite and fairchildite) were identified from wood ash.[26] Based on thermodynamic considerations,[22] $K_2Ca(CO_3)_2$ can be formed between 300 and 550 °C, whereas $K_2Ca_2(CO_3)_3$ is formed over 550 °C. However, the latter is unstable and decomposes to bütschliite and $CaCO_3$.[22,26] From the previously reported data, the following reactions (eqs 2−5) likely occurred during sample incineration at temperatures up to 600 °C in this study:

$$CaC_2O_4 \cdot H_2O \rightarrow CaC_2O_4 + H_2O \ (100-200°C) \quad (2)$$

$$2KHCO_3 \rightarrow K_2CO_3 + CO_2 + H_2O \ (100-200°C) \quad (3)$$

$$CaC_2O_4 \rightarrow CaCO_3 + CO \ (300-600°C) \quad (4)$$

$$CaCO_3 + K_2CO_3 \rightarrow K_2Ca(CO_3)_2 (300-600°C) \quad (5)$$

Most of the components detected in the raw and ash samples (Figure 8A−C) are evidently water-soluble, as there are no detectable K-containing components in the residue after the first extraction step (E1) using water as a solvent. The main component remaining in the residue after E1 for raw samples (Figure 8A) was an unchanging form of CaC_2O_4, whereas the postextraction residues of ash samples were dominated by $CaCO_3$ (Figure 8B,C). Similar observations were reported by Maeda et al.,[27] who studied the ash from woody biomass combustion and found that the K component comprised relatively small particles composed of crystallized hydro-soluble K compounds (e.g., KCl and K_2SO_4). The XRD spectrum for

residues after water extraction was similar to that observed in this study, i.e., dominated by the $CaCO_3$ fraction.

In contrast to K-containing compounds, it is not possible to detect Mn-containing compounds using XRD. Therefore, the Mn compounds in raw and ash samples (300 and 600 °C) were analyzed using Mn K-edge XANES spectroscopy (Figure 9). In the raw-sample spectra (Figure 9A), a small pre-edge peak (a), a sharp, high-intensity peak (b), and a broad shelf on the high-energy side (c) were observed at 6538, 6550, and 6595 eV, respectively. Upon comparison with selected reference data, evident similarities with the spectral shapes for $MnCl_2 \cdot 4H_2O$ and $MnSO_4 \cdot 5H_2O$ (sharp, high-intensity peaks) could be seen, indicating that Mn in the raw samples predominantly had a divalent charge. These results were similar to those of Fernando et al.,[28] who studied the Mn structures in Mn-hyperaccumulating plants in detail and reported that among the divalent forms of Mn, foliar Mn was predominant and formed complexing ligands with carboxylic acids. Mn(II) was also found to be the predominant form in wood.[29] This explains the estimated extraction efficiency for Mn (33−38%) from raw samples using water (Figure 4) e.g., the water solubilities of $MnCl_2$ and $MnSO_4$ are 723 and 520 g·L^{-1}, respectively.[30]

For ash samples obtained at 300 °C, the Mn K-edge energy levels (Figure 9B) exhibited an evident shift to the higher-energy range, which is associated with increasing valence in Mn forms.[31] The spectral patterns for the ash samples were similar to those for Mn_2O_3, a reference compound, with a high-intensity peak (b') observed at approximately 6556−6557 eV. The observed change indicated that Mn(II) had been mainly converted to Mn(III). Nevertheless, the broad shoulder of the b peak with its maximum value corresponding to the Mn(II) oxidative state indicated that some water-soluble Mn forms remained in ash generated at 300 °C. For ash samples obtained at 600 °C (particularly S3 and S5) (Figure 9C), the peak shifted from 6557 eV (b') to 6559 eV (b''). This could indicate changes within the electron configuration of Mn(IV).[32] Mn_2O_3 and Mn_3O_4 were

detected during the incineration (from 20 to 900 °C) of biomass with synthesized Mn(II)—organic acid complexes.[33] The oxides were formed from the intermediate products MnO and Mn_2OX_2 (where X = Cl or Br) in three degradation steps.

Mn(III) and Mn(IV) are not soluble in water,[30] which may explain why the Mn extraction efficiency decreases drastically after the first step (E1 with water), whereas newly formed Mn compounds are almost completely extracted with acid solvents in the second step (Figures 5B and 6B). Furthermore, the decrease in extraction efficiency of Mn from samples incinerated at high temperatures (500 and 600 °C) might have been due to the formation of more stable complexes with other elements present in the raw samples (Table 1). A broad-scale study on the composition of ash from various types of biomasses found that Mn usually coexists with Ca and Mg.[34] The most likely compounds are newly formed carbonates, oxyhydroxides, glass, silicates, and some phosphates and sulfates.[34,35]

4. CONCLUSIONS

In this study, we showed the feasibility of efficient extraction of K and Mn from ginger crop waste, using the raw and ash samples (as shown in Figure 1).

It was found that the K can be efficiently extracted (100%) using H_2O from raw samples; however, it was not possible to separate Mn, which tends to be extracted also in the amount of over 33% of its total content in the raw sample.

Incineration of the raw samples could effectively impact the extraction selectivity allowing for the separation of K from the Mn. Among the studied temperatures (100−600 °C), it was found that the most effective separation and efficient extraction of the K and Mn, was obtained from the ash received at 300 °C. The extraction of K was almost completed (∼96%) in the first step, using H_2O. In the second step, almost complete extraction (∼90%) of Mn was achieved using nitric acid solutions. Additionally, CA, a cost-effective and environmentally friendly solvent, was just as effective as HNO_3 in extracting Mn (∼85%).

Spectroscopic studies of the ashes received at 300 °C indicated that the Mn can change its oxidative state from Mn(II) (water-soluble) to Mn(III) and/or Mn(IV) (water-insoluble) (Figure 9B). The XRD (Figure 8) revealed that within K compounds, there were complex reactions associated with the changes mainly within carbonates but without a negative impact on the K extraction efficiency.

■ AUTHOR INFORMATION

Corresponding Author

Sylwia Oleszek − *Department of Environmental Engineering, Graduate School of Engineering, Kyoto University, 615-8540 Kyoto, Japan; Institute of Environmental Engineering of the Polish Academy of Sciences, 41-819 Zabrze, Poland;* ● orcid.org/0000-0001-6660-9992; Phone: +81-75-383-3335; Email: oleszek.sylwia.2r@kyoto-u.ac.jp; Fax: +81-75-383-3338

Authors

Kenji Shiota − *Department of Environmental Engineering, Graduate School of Engineering, Kyoto University, 615-8540 Kyoto, Japan*

Minhsuan Chen − *Department of Environmental Engineering, Graduate School of Engineering, Kyoto University, 615-8540 Kyoto, Japan*

Masaki Takaoka − *Department of Environmental Engineering, Graduate School of Engineering, Kyoto University, 615-8540 Kyoto, Japan;* ● orcid.org/0000-0002-6088-8326

Complete contact information is available at:
https://pubs.acs.org/10.1021/acsomega.2c02002

Author Contributions

The manuscript was written through the contributions of all authors. All authors have given approval to the final version of the manuscript

Notes

The authors declare no competing financial interest.

■ REFERENCES

(1) Hund, K.; La Porta, D.; Fabregas, T. P.; Laing, T.; Drexhage, J. *Minerals for Climate Action: The Mineral Intensity of the Clean Energy Transition*; International Bank for Reconstruction and Development/ The World Bank, 2020, www.worldbank.org.

(2) Elshkaki, A.; Graedel, T. E.; Ciacci, L.; Reck, B. K. Resource Demand Scenarios for the Major Metals. *Environ. Sci. Technol.* **2018**, *52*, 2491−2497.

(3) Critical Mineral Resources of the United States-Economic and Environmental Geology and Prospects for Future Supply. In *Manganese*; Cannon, W. F.; Kimball, B. E.; Corathers, L. A.; Schulz, K. J.; DeYoung, J. H., Jr.; Seal, R. R., II.; Bradley, D. C., Eds.; U.S Geological Survey: U.S, 1802; Vol. *2017*, pp L1−L28, DOI: 10.3133/ pp1802L.

(4) Drexhage, J. *The Growing Role of Minerals and Metals for a Low Carbon Future*; International Bank for Reconstruction and Development/The World Bank, 2017, www.worldbank.org.

(5) Sun, X.; Hao, H.; Liu, Z.; Zhao, F. Insights into the global flow pattern of manganese. *Resour. Policy* **2020**, *65*, No. 101578.

(6) Grygo-Szymanko, E.; Tobiasz, A.; Walas, S. Speciation analysis and fractionation of manganese: A review. *TrAC, Trends Anal. Chem.* **2016**, *80*, 112−124.

(7) Bidwell, S. D.; Woodrow, I. E.; Batianoff, G. N.; Sommer-Knudsen, J. Hyperaccumulation of manganese in the rainforest tree *Austromyrtus bidwillii* (Myrtaceae) from Queensland, Australia. *Funct. Plant Biol.* **2002**, *29*, 899−905.

(8) Mizuno, T.; Asahina, R.; Hosono, A.; Tanaka, A.; Senoo, K.; Obata, H. Age-dependent manganese hyperaccumulation in *Chengiopanax sciadophylloides* (Araliaceae). *J. Plant Nutr.* **2008**, *31*, 1811−1819.

(9) Fernando, D. R.; Marshall, A.; Baker, A. J. M.; Mizuno, T. Microbeam methodologies as powerful tools in manganese hyperaccumulation research: present status and future directions. *Front. Plant Sci.* **2013**, *4*, 1−9.

(10) Juárez-Santillán, L. F.; Lucho-Constantino, C. A.; Vázquez-Rodríguez, G. A.; Cerón-Ubilla, N. M.; Beltrán-Hernández, R.I. Manganese accumulation in plants of the mining zone of Hidalgo, Mexico. *Bioresour. Technol.* **2010**, *101*, 5836−5841.

(11) Li, J. T.; Gurajala, H. K.; Wu, L. H.; van der Ent, A.; Qiu, R. L.; Baker, A. J. M.; Tang, Y. T.; Yang, X.; Shu, W. S. Hyperaccumulator plants from China: A synthesis of the currentstate of knowledge. *Environ. Sci. Technol.* **2018**, *52*, 11980−11994.

(12) Yang, Q.-w.; Ke, H.; Liu, S.; Zeng, Q. Phytoremediation of Mn-contaminated paddy soil by two hyperaccumulators (*Phytolacca americana* and *Polygonum hydropiper*) aided with citric acid. *Environ. Sci. Pollut. Res.* **2018**, *25*, 25933−25941.

(13) Lanzerstorfer, C. Potential of industrial de-dusting residues as a source of potassium for fertilizer production—A mini review. *Resour., Conserv. Recycl.* **2019**, *143*, 68−76.

(14) Mananda, A. B.; Harada, H.; Halem, H. I. A.; Mitoma, Y.; Keiko, F. Study of Potassium Recovery from Biomass Ash Using Tartaric Acid and Syngenite Method. *J. Mater. Sci. Chem. Eng.* **2021**, *09*, 39−52.

(15) Andrews, E. M.; Kassama, S.; Smith, E. E.; Brown, P. H.; Khalsa, S. D. S. A Review of potassium-rich crop residues used as organic matter amendments in tree crop agroecosystems. *Agriculture* **2021**, *11*, No. 580.

(16) Food and Agriculture Organization of the United Nations, *World Fertilizer Trends and Outlook to 2020, Summary Report*; FAO: Rome, 2017.

(17) Food and Agriculture Organization of the United Nations, *World Fertilizer Trends and Outlook to 2022*; FAO: Rome, 2019.

(18) Qin, J.; Yu, C.; Nie, H.; Li, L.; Luo, Z.; Zuo, K. The effect of temperature on transformation and release of potassium during the straw combustion. *ACTA Energiae Solaris Sinica* **2010**, *5*, 540−544.

(19) Wang, Y.; Wang, X.; Tan, H.; Du, W.; Qu, X. Extraction and quantitation of various potassium salts in straw ash. *Environ. Prog. Sustainable Energy* **2015**, *34*, 333−338.

(20) Samadhi, T. W.; Wulandari, W.; Amalia, R. A.; Khairunnisah, R. Potassium recovery from tropical biomass ash. *AIP Conf. Proc.* **2019**, *2085*, No. 020003.

(21) Mizuno, T.; Emori, K.; Ito, S. Manganese hyperaccumulation from noncontaminated soil in *Chengiopanax sciadophylloides* Franch. et Sav. and its correlation with calcium accumulation. *Soil Sci. Plant Nutr.* **2013**, *59*, 591−602.

(22) Thyrel, M. Spectroscopic Characterization of Lignocellulosic Biomass. Doctoral Thesis, Swedish University of Agricultural Sciences: Umeå, Sweden, 2014.

(23) Kostas, N. Woody Biomass Combustion at Slow and High Heating Rates: Effect of Manganese Dioxide on Biomass Combustion. Master Thesis, Delft University of Technology: Delft, Netherlands, 2017.

(24) Deka, D. C.; Neog, S.R. *Agricultural Benefits of Postharvest Banana Plants*; Bentham Science Publisher, Pte. Ltd.: Singapore, 2021; p 978, 981-18-0163-1.

(25) Sugiura, C.; Muramatsu, S. K-Edge X-Ray Absorption Spectra from Potassium Compounds. *Phys. Status Solidi B* **1985**, *132*, K111−K115.

(26) Navrotsky, A.; Putnam, R. L.; Winbo, C.; Rose, E. Thermochemistry of double carbonates in the K_2CO_3-$CaCO_3$ system. *Am. Mineral.* **1997**, *82*, 546−548.

(27) Maeda, N.; Fukasawa, T.; Katakura, T.; Ito, M.; Ishigami, T.; Huang, A. N.; Fukui, K. Existence form of potassium components in woody biomass. Combustion ashes and estimation method of its enrichment degree. *Energy Fuels* **2018**, *32*, 517−524.

(28) Fernando, D. R.; Mizuno, T.; Woodrow, I. E.; Baker, A. J. M.; Collins, R.N. Characterization of foliar manganese (Mn) in Mn (hyper)accumulators using X-ray absorption spectroscopy. *New Phytol.* **2010**, *188*, 1014−1027.

(29) Zelinka, S. L.; Jakes, J. E.; Kirker, G. T.; Bishell, A. B.; Boardman Ch, R.; Lai, B.; Sterbinsky, G. E.; Jellison, J.; Goodell, B. Oxidation states of iron and manganese in lignocellulose altered by the brown rot fungus *Gloeophyllum trabeum* measured in-situ using X-ray absorption near edge spectroscopy (XANES). *Int. Biodeterior. Biodegrad.* **2021**, *158*, No. 105162.

(30) Howe, P. D.; Malcolm, H. M.; Dobso, S. Manganese and Its Compounds: Environmental Aspects. In *Concise International Chemical Assessment Document 63*; WHO: Geneva, 2004, https://apps.who.int/iris/handle/10665/42992.

(31) Chalmin, E.; Farges, F.; Brown, G.E., Jr A pre-edge analysis of Mn K-edge XANES spectra to help determine the speciation of manganese in minerals and glasses. *Contrib. Mineral. Petrol.* **2009**, *157*, 111−126.

(32) Glatzel, P.; Bergmann, U.; Yano, J.; Visser, H.; Robblee, J. H.; Gu, W.; de Groot, F. M. F.; Christou, G.; Pecoraro, V. L.; Cramer, S. P.; Yachandra, V.K. The electronic structure of Mn in oxides, coordination complexes, and the oxygen-evolving complex of photosystem II studied by resonant inelastic X-ray Scattering. *J. Am. Chem. Soc.* **2004**, *126*, 9946−9959.

(33) Drzewiecka-Antonik, A.; Ferenc, W.; Mirosław, B.; Osypiuk, D.; Sarzyński, J. Structure, thermal stability and magnetic behavior of Mn(II) complexes with phenoxyacetic acid herbicides. *Polyhedron* **2021**, *207*, No. 115370.

(34) Vassilev, S. V.; Baxter, D. n overview of the behaviour of biomass during combustion: Part II. Ash fusion and ash formation mechanisms of biomass types. *Fuel* **2014**, *117*, 152−183.

(35) Vassilev, S. V.; Baxter, D. n overview of the behaviour of biomass during combustion: Part I. Phase-mineral transformations of organic and inorganic matter. *Fuel* **2013**, *112*, 391−449.

📖 **Recommended by ACS**

Enhanced Leaching of Mn from Electrolytic Manganese Anode Slime via an Electric Field

Yong Yang, Xianquan Ming, *et al.*
NOVEMBER 22, 2021
ENERGY & FUELS   READ ⧉

Clean Stepwise Extraction of Valuable Components from Electrolytic Manganese Residue via Reducing Leaching–Roasting

Xuli Li, Haobo Hou, *et al.*
JUNE 10, 2021
ACS SUSTAINABLE CHEMISTRY & ENGINEERING   READ ⧉

Eco-Friendly Organic Acid-Assisted Mechanochemical Process for Metal Extraction from Spent Lithium-Ion Batteries

Li Cai, Li Li, *et al.*
AUGUST 04, 2022
ACS SUSTAINABLE CHEMISTRY & ENGINEERING   READ ⧉

Sustainable Valuable Metal Recovery from the V–Cr–Fe Ternary Slime via Leaching-Selective Complexation

Yang Zhang, Wei Jin, *et al.*
DECEMBER 23, 2019
ACS SUSTAINABLE CHEMISTRY & ENGINEERING   READ ⧉

Get More Suggestions >